Electronic Supplementary Information for

Interfacial modification of Zn foil electrode with cationic surfactants enables efficient and selective CO production from CO_2 electroreduction

Hui Pan, Fang Wang, Zhengguo Zhang and Shixiong Min*

School of Chemistry and Chemical Engineering, North Minzu University, Yinchuan, 750021, P. R. China.

*Corresponding authors: sxmin@nun.edu.cn

1. Experimental

1.1 Chemicals and reagents

All chemicals used in this work were of analytical grade and used without further purification. Zinc foil (99.99%, thickness: 0.3 mm) was purchased from Tengfeng Metal Materials Co., Ltd. Cetyltrimethylammonium bromide (CTAB, 99%) and potassium bicarbonate ($KHCO_3$, 99.5%) were obtained from Aladdin Industrial Co., Ltd. Potassium bromide (KBr, 99.0%), tetradecyltrimethylammonium bromide (TTAB, 99%) and octadecyl trimethylammonium bromide (OTAB 99%) were purchased from Shanghai Titan Technology Co., Ltd. The CO_2 (99.999%) was purchased from Jinghua Industrial Gas Co., Ltd. Nafion 117 membrane was provided by Alfa Aesar Chemical Co., Ltd. Ultrapure water (18.2 MΩ cm) obtained from a water purification system (Hitech ECO-S15) was used in all experiments.

1.2 Pretreatment of Zn foil

A piece of zinc foil (1.0 cm×1.5 cm) was mechanically polished with sandpaper (2000 mesh) to remove the natural oxide layer, and then successively washed with acetone, water and ethanol, and finally dried under a flow of N_2 at room temperature.

1.3 Electrochemical measurements

The electrochemical CO_2 reduction experiments were performed in a H-type cell separated by a Nafion 117 membrane with a CHI660E electrochemical workstation (CH Instruments, Inc., Shanghai). An Ag/AgCl (in a saturated KCl solution) and a Pt coil were used as the reference electrode and the counter electrode, respectively, and CO_2-saturated 0.1 M $KHCO_3$ (pH=7.2) was used as electrolyte. All the applied potentials were reported as revisable hydrogen electrode (RHE) potentials scale using *E* (*vs*. RHE) =*E* (*vs.* Ag/AgCl) +0.656 V–iR_s. The reference electrode was calibrated with a Pt coil as the working electrode for the reversible hydrogen potential in the electrolyte solution purged with N_2 for 30 min and saturated high purity H_2 prior to the measurements. The cyclic voltammetry (CV) was run at a scan rate of 1 mV s^{-1}, and the average of the two potentials at which the current crossed zero was taken to be the thermodynamic potential for the hydrogen electrode reactions.[1] Liner sweep voltammetry (LSV) measurements for the electrodes was carried out in were performed N_2- or CO_2-bubbled 0.1 M $KHCO_3$ solution with a scan rate of 1 mV s^{-1}. For the bulk CO_2 electrolysis, the cathodic compartment was purged with CO_2 (99.999%) at a constant rate of 10 mL min^{-1}. The gas effluent from the cathodic compartment was delivered directly to the sampling loop of an on-line pre-calibrated gas chromatograph (PANNA GC-A91 plus) equipped with a thermal conductivity detector (TCD) and a flame ionization detector (FID). Faradaic efficiency (FE) of gaseous products at each applied potential was calculated based on following equation:

$$FE_i = \frac{Z_i \times G \times V_i \times t \times p_0 \times F \times 10^{-3}}{Q_{total} \times R \times T_0} \times 100\%$$

where Z is the number of electrons transferred (for CO and H_2 production; *Z*=2); *G* is volumetric flow rate (10 mL min^{-1}); V_i is the volume ratio of gas product i; t is reaction time (min); P_O and T_O are atmospheric pressure (101.3 KPa) and reaction temperature (298.15 K); respectively. *F* is faradaic constant (96485 C mol^{-1}); Q_{total} is integrated charge at each applied potential and *R* is ideal gas constant (8.314 J·mol^{-1} K^{-1}).

At the end of the electrolysis, the liquid products were analyzed by a highperformance liquid chromatography (HPLC) (HITACHI).

Electrochemical impedance spectroscopy (EIS) measurements were performed in a CO_2-bubbled 0.1 M $KHCO_3$ solution at open circuit voltage in the absence and presence of CTAB at different polarization potentials. The Nyquist plots were fitted with an equivalent circuit, where R_E is the solution resistance, R_{CT} is the charge transfer resistances, and CPE is the constant phase element.[1] Double layer capacitance (C_{dl}) value has been calculated using the equation as follows and the same Zn electrode was used to ensure similar surface roughness.

$$C_{dl} = \left\{ {R_{CT}}^{(1-N)} CPE \right\}^{(1/N)}$$

Cyclic voltammetry (CV) tests were performed in CO_2-purged 0.05 M $K_3[Fe[(CN)_6]$ solution (0.1 M $KHCO_3$ as supporting electrolyte) to determine the electrochemically active surface areas (ECSAs) of the Zn foil electrode with or without CTAB addition.[2-4]In this system, the relationship between the peak current value $[(i_{pc}+i_{pa})/2]$ and the square root of the scan rate ($v^{1/2}$) can be described by the Randles-Sevcik equation:

$$i_p = 2.69 \times 10^5 n^{3/2} A D^{1/2} v^{1/2} C$$

where i_p is the peak current value (A); n is the number of electron transfer; A is the ESCA of the electrode (cm^2); D is the diffusion coefficient ($cm^2\ s^{-1}$); C is the concentration of $K_3[Fe[(CN)_6]$ ($mol\ cm^{-3}$); v is the scanning speed ($V\ s^{-1}$).

1.4 Characterization

X-ray powder diffraction (XRD) was performed with a Rigaku smart lab diffractometer operated at 40 kV and 40 mA with nickel filtrated Cu $K\alpha$ radiation. X-ray photoelectron spectroscopy (XPS) analysis were performed using Thermo

Scientific ESCALAB 250Xi instrument. The instrument was equipped with an electron flood and a scanning ion gun. All spectra were calibrated according to the C 1s binding energy at 284.8 eV. Scanning electron microscopy (SEM) and energy x-ray spectrometer (EDX) were performed using a field emission microscope (SIGMA 500) for analyze the morphology and composition of the catalyst. Raman spectra of the electrodes were collected by using a Thermo Fisher DXR Raman spectrometer with a 780 nm laser as an excitation source.

2. Computational method

All calculations were performed through the spin-polarized density functional theory method by using the Vienna Ab-initio Simulation Package (VASP) based on the plane-wave pseudopotential. A plane-wave energy cutoff was set to be 400 eV. Zn (101) surface was modelled by (3×4) atomic supercell, A vacuum slab of 15 Å was built along z direction in each model to prevent interactions between periodic repeating structures. According to the Monkhorst-Pack scheme, a gamma-oriented (4×4×1) k-point grid is used for the Brillouin zone integration of the slabs. Additionally, the dipole correction was applied along the z-direction and the top two layers of Zn slabs were only allowed to relax while one bottom layer was fixed to describe the bulk characteristics of Zn crystal.

All atomic structures were optimized until the forces less than 0.03 eV Å^{-1}. For the adsorption models, all possible adsorption sites were calculated but the most stable adsorption site was only considered for the free energy calculation. Maximum atomic force of 0.05 eV was chosen as the convergence criterion for structure relaxation. The free energy of adsorbates and non-adsorbed gas-phase molecules is calculated as

$$G = E_{elec} + E_{ZPE} + \Delta H + (0 \rightarrow T) + T\Delta S = E_{elec} + G_{(T)}$$

The E_{elec} is the reaction energy of the elementary reaction obtained by DFT calculations, E_{ZPE} is the zero-point energy estimated under harmonic approximation by taking the vibrational frequencies of adsorbates or molecules as calculated within DFT. The entropies of H_2 (g), CO_2 (g) and CO (g) at 1 atm are used, while the entropy of H_2O (l) is calculated at 0.035 atm, which corresponds to the vapor pressure of liquid water at 298.15 K. Due to the use of PBE functional, the non-adsorbed gas-phase CO molecule has to include a -0.51 eV correction.

3. Addition data

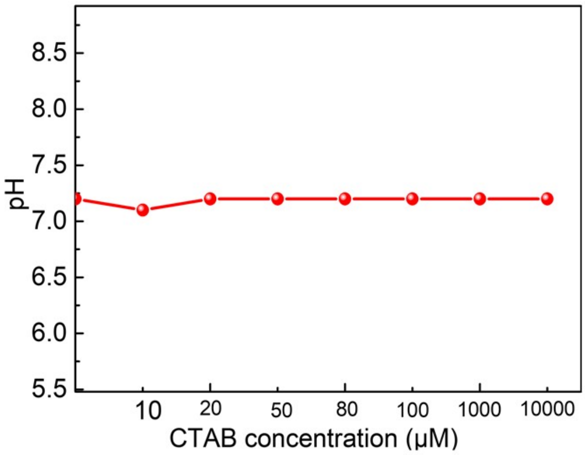

Fig. S1 The pH value of a CO_2-bubbled 0.1 M $KHCO_3$ solution with addition of CTAB with different concentrations.

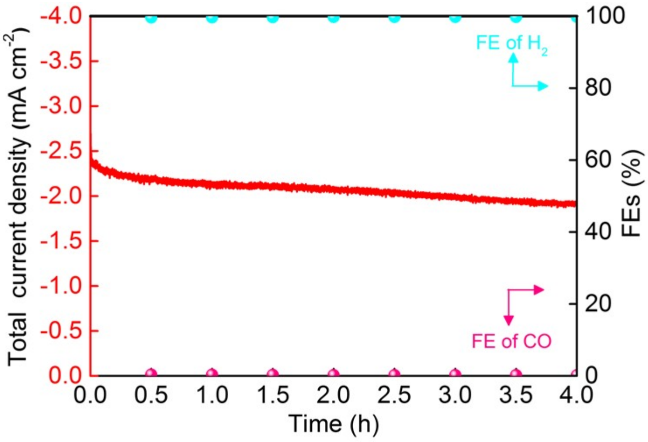

Fig. S2 CO_2 reduction on Zn foil electrode in a N_2-bubbled 0.1 M $KHCO_3$ solution containing 50 μM CTAB at -0.9 V vs. RHE.

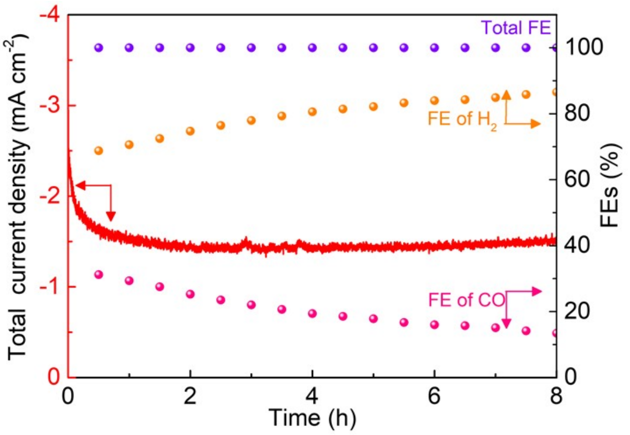

Fig. S3 Stability of CO_2RR on pristine Zn foil electrode at -0.9 V *vs*. RHE.

Table S1 Comparison of electrocatalytic performances of Zn-based catalysts for CO_2 reduction.

Zn-based catalysts	Electrolyte	Potential (V *vs.* RHE)	j_{CO} (mA cm^{-2})	FE_{CO}	Ref.
Porous Zn	0.5 M $KHCO_3$	-0.9	~6.6	77.8%	5
Zn/carbon/Ag	0.5 M $KHCO_3$	-1.0	~7.3	86%	6
Multilayered Zn nanosheets	0.5 M $NaHCO_3$	-1.13	~7.8	86%	7
Commercial Zn foil	0.1 M $KHCO_3$	-1.3	~4.1	78.9	8
Porous Zn	0.1M $KHCO_3$	-0.8	~1.2	81%	9
Ag-decorated Zn nanoplates	0.1 M $KHCO_3$	-0.8	~4.9	84%	10
Hexagonal Zn nanoplates	0.1 M $KHCO_3$	-0.96	~6	94.2%	11
ZnS/Zn/ZnS	0.1 M $KHCO_3$	-0.8	~9	94.2%	12
Nanoscale Zn	0.5 M NaCl	-1.6	~2.2	93%	13
Zn foil	0.1M $KHCO_3$ (CTAB)	-0.9	~4.89	94%	This work

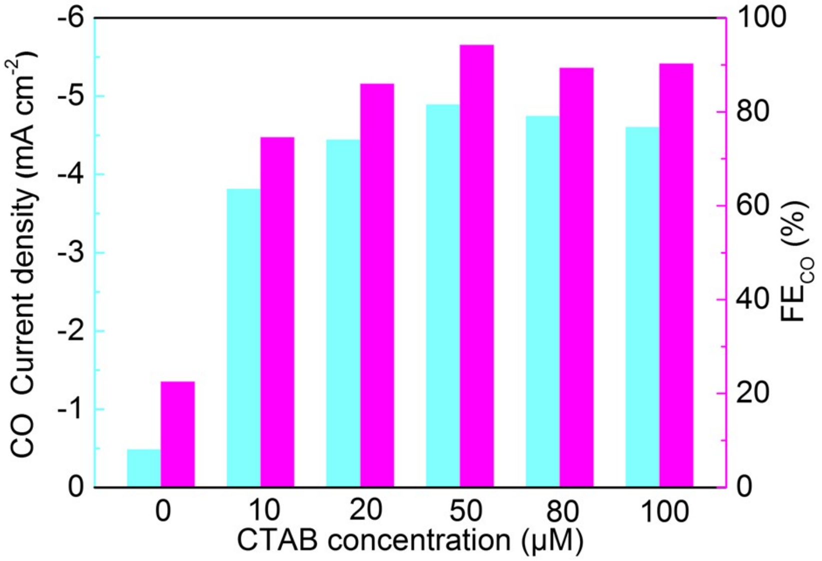

Fig. S4 FE_{CO} and CO current density as a function of CTAB concentration at −0.9 V *vs*. RHE.

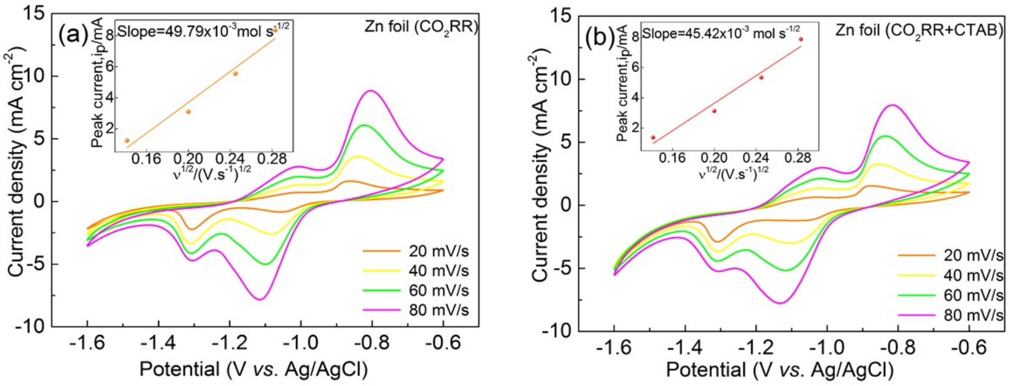

Fig. S5 Cyclic voltammetry curves (CV) measured in a CO_2-bubbled 0.1 M $KHCO_3$ solution containing 0.05 M $K_3[Fe[(CN)_6]$ using a Zn foil electrode after CO_2RR (a) without and (b) with CTAB addition (50 μM). The insets in panels a and b are the curves of the peak current ($(i_{pc}+i_{pa})/2$) as a function of square root of the scan rate ($v^{1/2}$).

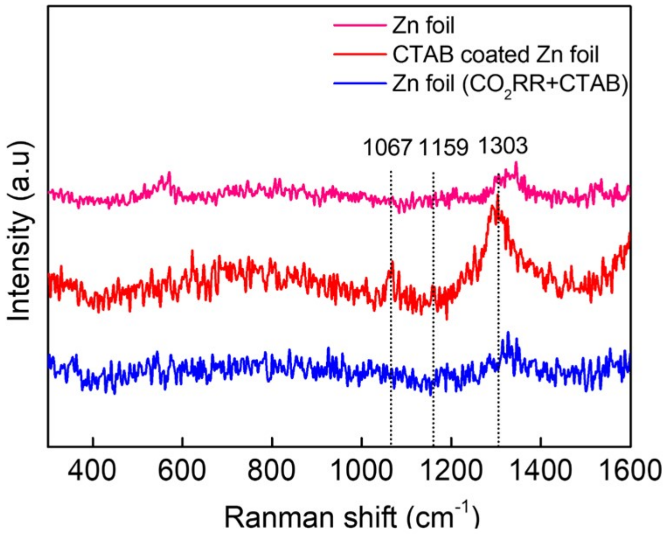

Fig. S6 Raman spectra pristine Zn foil, CTAB coated Zn foil (prepared by drop-casting CTAB on Zn foil serveing as the reference), and Zn foil after CO_2RR with CTAB addition.

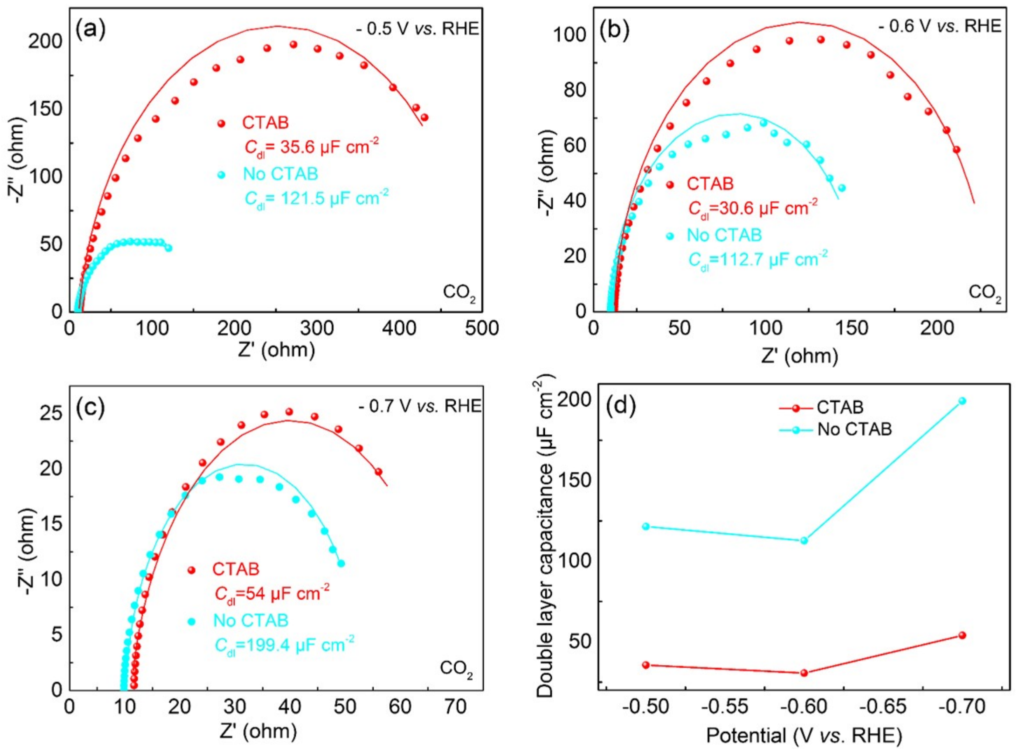

Fig. S7 EIS plots measured at (a) -0.5 V, (b) -0.6 V, and (c) -0.7 V *vs*. RHE in a CO_2-bubbled 0.1 M $KHCO_3$ solution in the presence and absence of 10 mM CTAB. (d) Double-layer capacitance extracted by fitting EIS impedance data.

Table S2 Zero-point energy corrections and free energy for various system.

System	E (eV)	G_{ZPE} (eV)	G (eV)
Zn/TMAB	-190.65	4.01	-186.64
Zn/TMAB-COOH	-216.77	4.60	-212.17
Zn/TMAB-CO	-205.99	4.19	-201.79
Zn	-97.61	-	-97.61
Zn-COOH	-124.44	0.51	-123.92
Zn-CO	-113.99	0.08	-113.90
H_2	-6.76	-0.05	-6.81
CO_2	-22.99	-0.26	-23.25
H_2O	-14.22	0	-14.22
CO	-14.80	-0.39	-15.70

References

1. S. Banerjee, X. Han and V. S. Thoi, *ACS Catal*., 2019, **9**, 5631-5637.

2. X. L. Cui, Q. Zhao, Z. Z. Li, Z. Y. Sun and Z. Y. Jiang, *Nanotechnology,* 2007, **18**, 215701.

3. H. Y. Shang, S. K. Wallentine, D. M. Hofmann, Q. Zhu, C. J. Murphy, L. R. Baker, *Chem. Sci.,* 2020, **11**, 12298-12306.

4. K. K. Diao, Z. Xiao and Y. Y. Zhao, *Mater. Chem. Phys.,* 2015, **162**, 571-579.

5. D. L. Nguyen, M. S. Jee, D. H. Won, H. Jung, H. S. Oh, B. K. Min and Y. J Hwang, *ACS Sustainable Chem. Eng*., 2017, **5**, 11377-11386.

6. F. Yang, P. Song, X. Liu, B. Mei, W. Xing, Z. Jiang, L. Gu and W. Xu, *Angew. Chem. Int. Ed*., 2018, **57**, 12303-12307.

7. T. Zhang, X. Li, Y. Qiu, P. Su, W. Xu, H. Zhong and H. Zhang, *J. Catal*., 2018, **357**, 154-162.

8. Z. Chen, K. Mou, S. Yao and L. Liu, *ChemSusChem*, 2018, **11**, 2944-2952.

9. M. Morimoto, Y. Takatsuji, K. Hirata, T. Fukuma, T. Ohno, T. Sakakura and T. Haruyama, *Electrochim. Acta*, 2018, **290**, 255-261.

10. Q. Yu, X. Meng, L. Shi, H. Liu and J. Ye, *Chem. Commun*., 2016, **52**, 14105-14108.

11. J. Xiao, M. R. Gao, S. B. Liu and J. L. Luo, *ACS Appl. Mater. Interfaces*, 2020, **12**, 31431-31438.

12. C. Li, G. Shen, R. Zhang, D. Wu, C. Zou, T. Ling, H. Liu, C. Dong and X.-W. Du, *J. Mater. chem. A*, 2019, **7**, 1418-1423.

13. F. Quan, D. Zhong, H. Song, F. Jia and L. Zhang, *J. Mater. Chem. A*, 2015, **3**, 16409-16413.